Elastic constants of multidomain LiTa03 crystal

doi: 10.1063/1.371211

Elastic constants of multidomain $LiTaO_3$ crystal

Izumi Takanaga and Jun-ichi Kushibiki
Department of Electrical Engineering, Tohoku University, Sendai 980-8579, Japan

(Received 22 March 1999; accepted for publication 14 June 1999)

All the independent components of the elastic constant tensor of multidomain $LiTaO_3$ crystal were determined by measuring bulk acoustic wave velocities and density for five multidomain $LiTaO_3$ substrates perfectly depoled by heat treatment. Comparing these determined constants with the elastic constants of single-domain $LiTaO_3$ crystal revealed that the elastic constants of multidomain crystal c_{ij} differ from both the elastic constants at constant electric field c_{ij}^E and those at constant electric displacement c_{ij}^D for single-domain crystal. The angular dependences of leaky surface acoustic wave velocity were measured on single and multidomain 36° Y-cut $LiTaO_3$ substrates by line-focus-beam acoustic microscopy and compared with the calculated results using the determined constants. The measured results agreed well with the calculated results. The constants will be used to enhance theoretical understanding of the elastic properties of residual multidomains. © *1999 American Institute of Physics.* [S0021-8979(99)07318-1]

I. INTRODUCTION

Line-focus-beam (LFB) acoustic microscopy has been applied to the investigation of various materials and device fabrication processes. Substantial studies with this technology have been conducted on ferroelectric materials of $LiNbO_3$[1,2] and $LiTaO_3$[1,3] single crystals, which are widely used as substrates for surface acoustic wave (SAW) devices. The variations of elastic properties on/among substrates, which are mainly due to chemical composition changes and residual multidomains,[4,5] have been successfully detected as velocity changes of leaky surface acoustic waves (LSAWs).[6–8]

In particular, the LSAW velocity changes due to residual multidomains have been studied on $LiTaO_3$ substrates for SAW devices: X-cut 112.2° rotated Y propagating (X-112°Y) and 36° rotated Y-cut X-propagating (36°YX) substrates. The effects of residual multidomains on LSAW velocity variations obtained in the measurement on X-112°Y $LiTaO_3$ substrates for Rayleigh-type SAW devices have been quantitatively explained by comparing the LSAW velocities measured for two types of substrates with extremely different domain structures, the single- and the multidomain substrates.[7] However, the same method is not suitable for explaining the LSAW velocity changes obtained on 36°YX-$LiTaO_3$ substrates for shear horizontal (SH)-type SAW devices, as a Rayleigh-type mode of SAWs, which is nearly uncoupled with piezoelectricity, is used for characterization.[8] Considering the fact that the residual multidomain state is between the single- and multidomain states, information on the elastic properties of multidomain crystal as well as single-domain crystal is essential to quantitatively analyze LSAW velocity variations caused by residual multidomains.

In a recent study on single- and multidomain crystals of $LiTaO_3$, a comparison of the measured sound velocities of bulk acoustic waves in the X, Y, and Z-axis propagation directions revealed that their elastic properties considerably differ from each other.[9]

In this article, bulk acoustic wave velocities and density are measured on five multidomain $LiTaO_3$ substrates perfectly depoled by heat treatment, and all the independent components of the elastic constants of multidomain $LiTaO_3$ crystal are determined. In addition, angular dependences of LSAW velocity are measured on single- and multidomain 36° Y-cut $LiTaO_3$ substrates and compared with the calculated results using these determined constants.

II. PROCEDURE OF DETERMINING ELASTIC CONSTANTS

The multidomain $LiTaO_3$ crystal substrates used in this article and the commercially available single-domain $LiTaO_3$ crystal substrates are extremes in domain structure. The latter are produced by heating grown crystals above the Curie temperature, and gradually cooling them with applying a dc electric field; they have a uniform spontaneous polarization. The crystals are then processed into substrates or wafers. The former are prepared by heating single-domain substrates above the Curie temperature and gradually cooling them without applying a dc electric field; these have antiparallel spontaneous polarizations. The domain size of a multidomain $LiTaO_3$ crystal is approximately 1 μm and much smaller than the wavelengths (15–65 μm) in the measurement frequency range (60–225 MHz), so the multidomain $LiTaO_3$ crystal substrates have no piezoelectricity. Considering that a single-domain $LiTaO_3$ crystal belongs to class $3m$ of the trigonal system, a multidomain $LiTaO_3$ crystal is treated as one belonging to nonpiezoelectric crystal of class $\bar{3}m$ in investigating the propagation of acoustic waves. Six independent elastic constants [$c_{11}(=c_{12}+2c_{66})$, c_{12}, c_{13}, c_{14}, c_{33}, and c_{44}] and density (ρ) are related with the propagation of acoustic waves.

These constants are determined by six bulk acoustic wave velocities and densities. For bulk waves which propa-

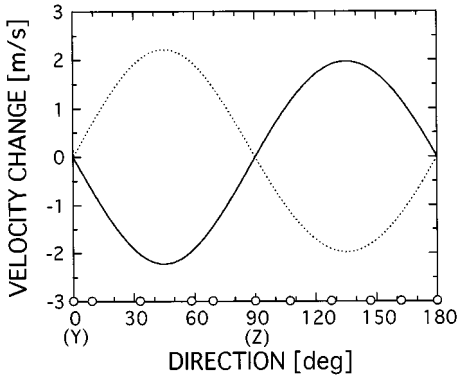

FIG. 1. X-polarized shear velocity changes influenced by 1% increase and decrease of the published constant c_{14}^E (see Ref. 10). Solid line: +1%, Dotted line: −1%. ○: angles of the crystalline planes described in ASTM card.

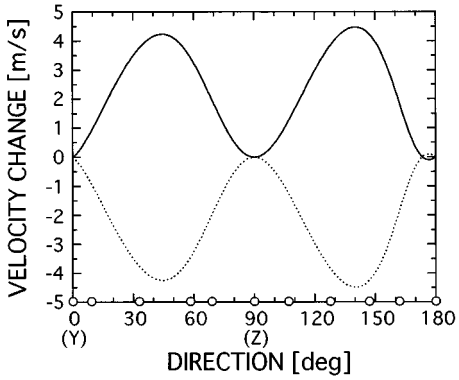

FIG. 2. Longitudinal velocity changes influenced by 1% increase and decrease of the published constant c_{13}^E (see Ref. 10). Solid line: +1%, Dotted line: −1%. ○: angles of the crystalline planes described in ASTM card.

gate along the X, Y, and Z axis, the equations between acoustic velocity V and elastic constant c_{ij} are simply expressed as follows:

$$c_{11}=\rho V_{Xl}^2, \tag{1}$$

$$c_{33}=\rho V_{Zl}^2, \tag{2}$$

$$c_{44}=\rho V_{Zs}^2, \tag{3}$$

$$c_{66}=\rho V_{YsX}^2. \tag{4}$$

V_{Xl} and V_{Zl} are the longitudinal velocities in the X- and Z-axis propagation directions, respectively. V_{Zs} is the degenerate shear velocity in the Z-axis propagation direction, and V_{YsX} is the X-polarized shear velocity in the Y-axis propagation direction. Using the velocities measured, the elastic constants of c_{11}, c_{33}, c_{44}, and c_{66} can be determined with Eqs. (1)–(4).

c_{14} is determined by the X-polarized shear velocity in the rotated Y-axis propagation direction, V_{rYsX}. The equation between c_{14} and V_{rYsX} is as follows:

$$c_{14}=(\rho V_{rYsX}^2-c_{44}\sin^2\theta-c_{66}\cos^2\theta)/\sin 2\theta. \tag{5}$$

θ is the rotation angle from the Y to Z axis. From this equation, c_{14} can be determined by using the determined c_{44} and c_{66} and the measured V_{rYsX}. The crystalline plane whose X-polarized shear velocity greatly depends on the constant to be determined, c_{14}, is selected as a specimen among crystalline planes described in the American Society for Testing and Materials (ASTM) card (No. 29-836). When employing a crystalline plane in the ASTM card, the inclination angle between the specimen surface and crystalline plane can be measured by x-ray analysis, and the propagation direction of acoustic waves can be recognized precisely. We examined the changes of X-polarized shear velocities in the rotated Y-axis propagation directions when c_{14}^E is changed ±1% by using the values in the literature.[10] The calculated results are shown in Fig. 1. Circles in the figure represent the angles of crystalline planes described in the ASTM card. The crystalline plane of $(02\bar{1}0)$ (rotated 58° Y-cut specimen) that shows the largest velocity change among the crystalline planes in the ASTM card is used for determining c_{14}.

Finally, c_{13} is determined by the longitudinal velocity of the rotated Y-cut specimen, V_{rYl}. The equation between the elastic constants and V_{rYl} is as follows:

$$(c'_{11}-\rho V_{rYl}^2)(c'_{66}-\rho V_{rYl}^2)-c'^2_{16}=0. \tag{6}$$

The primed constants indicate that the constants have been subjected to coordinate transformation for the desired propagation direction. All of c'_{11}, c'_{66}, and c'_{16} are functions of rotation angle θ and five elastic constants except c_{12}. From this equation, c_{13} can be determined by using the four determined elastic constants, c_{11}, c_{14}, c_{33}, and c_{44}, and the measured V_{rYl}. The propagation direction is selected by the calculations using the published values,[10] as well as c_{14}. The longitudinal velocity changes of the rotated Y-cut specimens when c_{13}^E is changed ±1% are shown in Fig. 2. In the angles of crystalline planes in the ASTM card, [306] (147° rotated Y axis), where the velocity change is maximum, is used for determining c_{13}.

III. MEASUREMENT METHODS AND RESULTS

The bulk acoustic wave velocity is measured by the double-pulse interference method using rf tone burst signals,[11] and the density is measured based on the Archimedes method.

Figure 3 shows the experimental arrangement of the velocity measurement. Two plane wave ultrasonic devices are

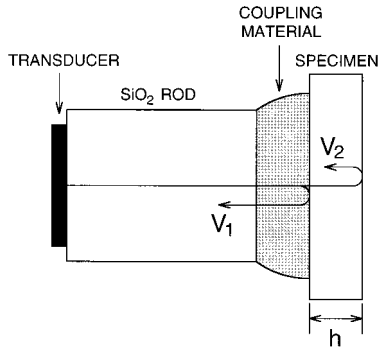

FIG. 3. Experimental arrangement of bulk-wave ultrasonic velocity measurements by the pulse interference method.

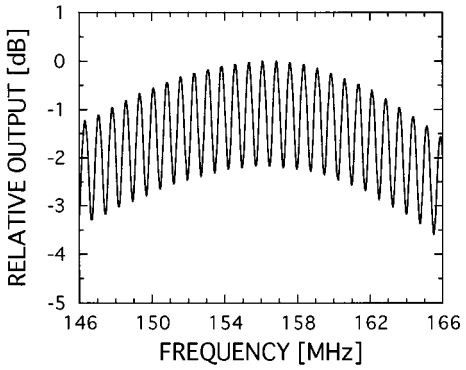

FIG. 4. Frequency response of the interference output for multidomain *Z*-cut $LiTaO_3$ specimen in longitudinal wave velocity measurement by the pulse interference method. The specimen thickness is 4038.2 μm.

prepared with a ZnO film transducer for longitudinal wave measurements and an *X*-cut $LiNbO_3$ transducer for shear wave measurements on cylindrical buffer rods of synthetic silica (SiO_2) glass. Coupling materials are pure water for longitudinal waves and a thin layer of bonding material salol (phenyl salicylate) for shear waves. The signals, which are converted into ultrasonic waves by the transducer, propagate through the buffer rod, coupling material, and specimen, as the waves are reflected and transmitted at each boundary and are reflected perfectly at the back surface of the specimen. Two reflected signals from the front surface of the specimen, V_1, and from the back surface, V_2, are superimposed in the time domain, and a typical interference wave form, as shown in Fig. 4, is obtained from the change in the phase difference between V_1 and V_2 by sweeping the frequency. The velocity V is determined with the frequency interval of the interference wave form, Δf, and the thickness of specimen, h, by the following equation:

$$V = 2\Delta f h. \tag{7}$$

The thickness of specimens is measured by a digital length gauging system with a precision of ± 0.1 μm. For shear velocity measurements, the reflected signals from the rod-salol boundary and from the salol-specimen boundary cannot be separated because the bonding layer of salol is very thin less than 1 μm. Therefore, the phase shifts caused by the transmissions and reflections at those boundaries affect the frequency interval. Shear velocity measurements are conducted by measuring the acoustic properties (velocity, attenuation coefficient, and density) of salol in advance, simulating the reflection coefficients and frequency intervals in the interference wave form based on the ultrasonic transmission line,[11] and fitting the simulated results to the experimental results. The inclination angles between the crystalline planes and specimen surfaces are measured for all specimens by x-ray analysis, and the velocity changes caused by these inclinations are corrected by calculations.

The densities of *Y*- and *Z*-cut specimens are measured to be $7460.5 \pm 0.4\,\mathrm{kg/m^3}$. The measured results for specimen thickness and velocity are shown in Table I. All measurements are carried out at temperatures around 23.0 °C. The measurement frequency range of longitudinal waves is 95 to 220 MHz, and that of shear waves is 60 to 180 MHz.

TABLE I. Measured results for specimen thickness and bulk wave velocity of the multidomain $LiTaO_3$ crystal.

Specimen	Mode	Thickness (μm)	Velocity (m/s)
X	Longitudinal wave	4069.1±0.1	5636.23±0.22
Z	Longitudinal wave	4038.2±0.1	6083.52±0.28
Z	Degenerate shear wave	4038.2±0.1	3713.85±0.39
Y	*X*-polarized shear wave	4049.3±0.1	3608.17±0.23
(02$\bar{1}$0) 58.35°Y	*X*-polarized shear wave	4040.4±0.1	3413.14±0.17
(30$\bar{6}$) 147.02°Y	Longitudinal wave	4014.0±0.1	5713.13±0.21

The determined elastic constants and density of multidomain $LiTaO_3$ crystal are shown in Table II, together with those of the single-domain crystal. Although the elastic constants of the single-domain crystal have been reported previously in several articles,[10,12–15] we adopt the constants determined from the single-domain specimens cut from the same ingot as the multidomain specimens used in this article to consider the differences in elastic properties between single- and multidomain crystals caused by the differences in domain structures.[16] The acoustical physical constants of the single-domain crystal (elastic constants at constant electric field c_{ij}^E, piezoelectric constants e_{ij}, dielectric constants at constant strain ϵ_{ij}^S, and density) are determined by measuring bulk longitudinal and shear velocities, dielectric constants, and density. Then, the elastic constants at constant electric displacement c_{ij}^D of the single-domain crystal are calculated by the following equation:[17]

$$c_{ij}^D = c_{ij}^E + e_{ik}(\epsilon^S)_{kl}^{-1} e_{lj}. \tag{8}$$

It is clear that the elastic constants of the multidomain $LiTaO_3$ crystal differ from both the elastic constants at constant electric field c_{ij}^E and those at constant electric displacement c_{ij}^D of the single-domain crystal. Although c_{13} of the multidomain crystal is almost equivalent to c_{13}^E of the single-domain crystal, the other elastic constants c_{ij} of multidomain crystal exist between c_{ij}^E and c_{ij}^D of the single-domain crystal. However, no significant difference in their density can be recognized.

TABLE II. Determined elastic constants and density of single and multidomin $LiTaO_3$ crystals.

		Single domain			Multidomain	
		c_{ij}^E	c_{ij}^D	c_{ij}	Difference from c_{ij}^E	Difference from c_{ij}^D
Elastic constant ($\times 10^{11}$ N/m^2)	c_{11}	2.331	2.421	2.370	+0.039	−0.051
	c_{12}	0.464	0.375	0.427	−0.037	+0.052
	c_{13}	0.835	0.827	0.835	0.000	+0.008
	c_{14}	−0.108	−0.237	−0.161	−0.053	+0.076
	c_{33}	2.752	2.845	2.761	+0.009	−0.084
	c_{44}	0.953	1.139	1.029	+0.076	−0.110
	c_{66}	0.933	1.023	0.971	+0.038	−0.052
Density ($\times 10^3$ kg/m^3)	ρ	7.4604		7.4605	+0.0001	

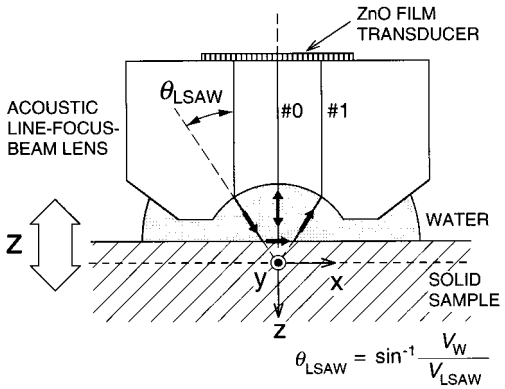

FIG. 5. A cross-section of the LFB acoustic lens to explain $V(z)$ curve measurements. θ_{LSAW}: critical angle of LSAW, V_{LSAW}: LSAW velocity, and V_W: longitudinal velocity in water.

IV. DISCUSSION

The angular dependences of LSAW velocity are measured at 225 MHz on single- and multidomain 36° Y-cut $LiTaO_3$ substrates by line-focus-beam (LFB) acoustic microscopy.

LFB acoustic microscopy is a technique used to measure the propagation characteristics of LSAWs propagating along the water-specimen boundary by analyzing $V(z)$ curves, which are obtained by changing the relative distance z between the ultrasonic device and the specimen.[18] A cross-sectional geometry of an ultrasonic device and a specimen is given in Fig. 5 to show the construction mechanism of a $V(z)$ curve. The ultrasonic device consists of a ZnO film piezoelectric transducer fabricated on the upper end of a Z-cut sapphire rod with a cylindrical concave surface at its base. When the relative distance between the ultrasonic device and the specimen, z, is varied, components Nos. 0 and 1 in Fig. 5 interfere, and an interference wave form called $V(z)$ curve is obtained, as shown in Fig. 6. From the oscillation interval in this wave form, Δz, LSAW velocity V_{LSAW} is given by the following equation:

$$V_{\mathrm{LSAW}}=\frac{V_W}{\sqrt{1-\left(1-\frac{V_W}{2f\Delta z}\right)^2}}, \tag{9}$$

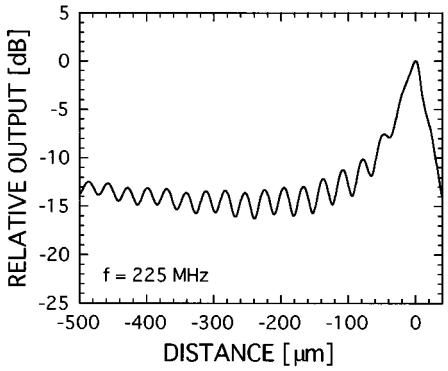

FIG. 6. $V(z)$ curve measured on a multidomain Z-cut $LiTaO_3$ specimen for Y-axis propagation.

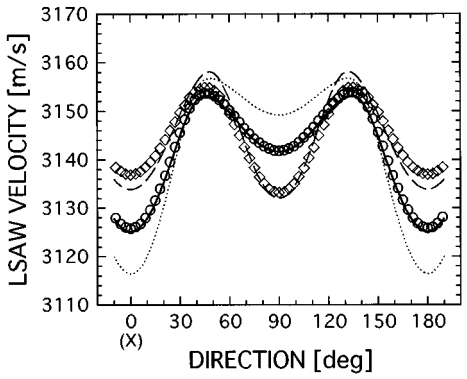

FIG. 7. Angular dependences of LSAW velocity measured on single- and multidomain 36° Y-cut $LiTaO_3$ substrates. ○: measured values for single-domain substrate. ◇: measured values for multidomain substrate. Solid line: results calculated using the determined constants for a single-domain crystal in Table II. Dashed line: results calculated using the determined constants for the multidomain crystal. Dotted line: results calculated using the published constants for the single-domain crystal (see Ref. 10).

where V_W is the sound velocity of longitudinal waves in water and f is the ultrasonic frequency. The measured values are calibrated by using gadolinium gallium garnet as a standard specimen whose elastic constants and density have been precisely measured.[19]

The measured results of the LSAW velocity for single- and multidomain 36° Y-cut $LiTaO_3$ substrates are shown in Fig. 7 together with the calculated results. Circles and diamonds are the measured values for single- and multidomain crystals, respectively. Solid and dashed lines are the results calculated by the determined constants of single- and multidomain crystals, respectively, and the dotted line is the result calculated by the published values for a single-domain crystal.[10] Although the measured LSAW velocities for the crystals used in this article cannot be explained by the dotted line with respect to the published values,[10] the measured values agree well with the values calculated by the determined constants for both single- and multidomain crystals.

V. CONCLUSION

In this article, bulk acoustic wave velocities and density were measured for multidomain $LiTaO_3$ substrates which are extremely different in the domain structure from the single-domain crystal, and all the independent components of the elastic constants were determined for the first time. Comparing the determined elastic constants of the multidomain $LiTaO_3$ crystal with those of the single-domain crystal revealed that the elastic constants of the multidomain crystal differ from both the elastic constants at constant electric field c_{ij}^E and those at constant electric displacement c_{ij}^D for the single-domain crystal. In addition, when the angular dependences of LSAW velocity were measured on single- and multidomain 36° Y-cut $LiTaO_3$ substrates by LFB acoustic microscopy and compared with the values calculated using the determined constants, the measured values agree well with the calculated values. The constants determined here will enable us to make theoretical calculations for interpre-

tations of the elastic properties of residual multidomains in $LiTaO_3$ crystal associated with acoustic inhomogeneities.

ACKNOWLEDGMENTS

The authors are grateful to M. Arakawa for his technical assistance in these experiments. This work was supported in part by a Research Grant-in-Aid from the Ministry of Education, Science, and Culture of Japan.

[1] A. A. Ballman, J. Am. Ceram. Soc. **48**, 112 (1965).
[2] J. R. Carruthers, G. E. Peterson, M. Grasso, and P. M. Bridenbaugh, J. Appl. Phys. **42**, 1846 (1971).
[3] S. Miyazawa and H. Iwasaki, J. Cryst. Growth **10**, 276 (1971).
[4] H. J. Levinstein, A. A. Ballman, and C. D. Capio, J. Appl. Phys. **37**, 4585 (1966).
[5] M. Sato, A. Iwama, J. Yamada, M. Hikita, and Y. Furukawa, Jpn. J. Appl. Phys., Suppl. **28-1**, 111 (1989).
[6] J. Kushibiki, H. Takahashi, T. Kobayashi, and N. Chubachi, Appl. Phys. Lett. **58**, 2622 (1991).
[7] J. Kushibiki, H. Takahashi, T. Kobayashi, and N. Chubachi, Appl. Phys. Lett. **58**, 893 (1991).
[8] J. Kushibiki, H. Ishiji, T. Kobayashi, N. Chubachi, I. Sahashi, and T. Sasamata, IEEE Trans. Ultrason. Ferroelectr. Freq. Control **42**, 83 (1995).
[9] J. Kushibiki and I. Takanaga, J. Appl. Phys. **81**, 6906 (1997).
[10] A. W. Warner, M. Onoe, and G. A. Coquin, J. Acoust. Soc. Am. **42**, 1223 (1967).
[11] J. Kushibiki, N. Akashi, T. Sannomiya, N. Chubachi, and F. Dunn, IEEE Trans. Ultrason. Ferroelectr. Freq. Control **42**, 1028 (1995).
[12] T. Yamada, H. Iwasaki, and N. Niizeki, Jpn. J. Appl. Phys. **8**, 1127 (1969).
[13] R. T. Smith and F. S. Welsh, J. Appl. Phys. **42**, 2219 (1971).
[14] G. Kovacs, M. Anhorn, H. E. Engan, G. Visintini, and C. C. W. Ruppel, Proc. 1990 IEEE Ultrasonics Symposium 1990, pp. 435–438.
[15] K. Taki and Y. Shimizu, Jpn. J. Appl. Phys., Part 1 **33**, 2976 (1994).
[16] J. Kushibiki, I. Takanaga, M. Arakawa, and T. Sannomiya, IEEE Trans. Ultrason. Ferroelectr. Freq. Control (in press).
[17] IEEE standard on piezoelectricity, Std 176-1987.
[18] J. Kushibiki and N. Chubachi, IEEE Trans. Sonics Ultrason. **SU-32**, 189 (1985).
[19] J. Kushibiki and M. Arakawa, IEEE Trans. Ultrason. Ferroelectr. Freq. Control **45**, 421 (1998).